fect. A particularly promising application for REX in this context concerns the study of light-driven (and other stimulus-driven) processes such as transduction in the membrane-associated visual pigment protein, rhodopsin.

REFERENCES AND NOTES

1. A. H. Compton and S. K. Allison, *X-Rays in Theory and Experiment* (Van Nostrand, New York, 1935).
2. L. G. Parratt, *Phys. Rev.* **95**, 359 (1954).
3. W. C. Marra, P. M. Eisenberger, A. Y. Cho, *J. Appl. Phys.* **50**, 6927 (1979).
4. R. S. Becker, J. A. Golovchenko, J. R. Patel, *Phys. Rev. Lett.* **50**, 153 (1983).
5. J. M. Bloch *et al.*, *ibid.* **54**, 1039 (1985).
6. P. M. Eisenberger and W. C. Marra, *ibid.* **46**, 1081 (1981).
7. M. J. Bedzyk, G. M. Bommarito, J. S. Schildkraut, *ibid.* **62**, 1376 (1989).
8. M. J. Bedzyk, D. H. Bilderback, G. M. Bommarito, M. Caffrey, J. S. Schildkraut, *Science* **241**, 1788 (1988).
9. M. J. Bedzyk, G. M. Bommarito, M. Caffrey, T. L. Penner, *ibid.* **248**, 52 (1990).
10. J. Wang, M. J. Bedzyk, T. L. Penner, M. Caffrey, *Nature* **354**, 377 (1991).
11. D. K. G. de Boer, *Phys. Rev. B* **44**, 498 (1991).
12. M. Born and E. Wolf, *Principles of Optics* (Pergamon, Oxford, ed. 6, 1991).
13. Labeling of the various incident (A), refracted or transmitted (T), and reflected (R) beams in the current two-interface system is shown in Fig. 2A. The subscripts, *ij*, refer to the media *i* and *j*. Thus, R_{ij} corresponds to the beam reflected back into medium *i* upon striking the $i \rightarrow j$ interface; A, T, and R also correspond to the amplitudes of the respective *E* fields. With the exception of A_{12}, all *E* field amplitudes are functions of incident angle and obey Fresnel theory (*1, 2, 12*). The transmission and reflection coefficients are defined by $r_{ij} = R_{ij}/A_{ij}$ and $t_{ij} = T_{ij}/A_{ij}$, respectively. The x-ray transmittance in medium 2 defined by
$$\alpha = \frac{A_{23}}{T_{12}} = \frac{A_{21}}{R_{23}}$$
is a complex factor which accounts for the attenuation and phase change of the x-ray beam traversing the medium.
14. For a given XSW period and the interface phase shift as described in (*7*), *n*th order resonance is observed when the incident angle θ_2 satisfies approximately the following relation
$$d = \frac{\lambda}{2\sin\theta_2}\left[n - \frac{1}{2} - \frac{1}{2\pi}\cos^{-1}\left(2\frac{\theta_2^2}{\theta_{c2}^2} - 1\right)\right]$$
where *d* is the thickness of medium 2.
15. According to (*14*), as medium 2 thins, the angle of incidence at which the resonance effect is observed increases. At the higher angles of incidence, however, the enhancement effect lessens because of a dramatic reduction in r_{21} and t_{12} (see Eq. 1). At the other extreme, where there is a thicker medium 2, the enhancement effect is less as a result of a reduction in transmittance, α, which is associated with a more profound attenuation of the x-ray beam in the thicker layer occurring at lower angles of incidence.
16. The term "roughly" is used to indicate that the alignment of troughs in the reflectivity curve with peaks and troughs in the fluorescence curve is not exact. The mismatch arises primarily because the probing heavy atom layer is placed slightly off the center position in medium 2.
17. G. M. Bommarito, thesis, Cornell University, Ithaca, NY (1987).
18. Because the thickness of the heavy atom probe layer is small (10 to 15 Å) compared to the width of the resonant *E* field intensity peak (~500 Å, Fig. 2B), the x-ray fluorescence is a reliable and a direct measure of the *E* field intensity at the position of the heavy atom probe layer in the adlayer with a spatial resolution of better than 20 Å. The mismatch in the height of the experimental and theoretical curves in Fig. 3A arises from nonuniformities in the organic thin film and from a finite divergence of the incident x-ray beam (~50 μrad full width at half maximum) not corrected for in the calculations.

19. This work was supported by grants from the National Institutes of Health (DK 36849 and DK 45295), a University Exploratory Research Program Award (Procter and Gamble Company), and a DuPont Young Faculty Award to M.C.; by separate grants from Eastman Kodak Company to M.J.B. and M.C.; and by a Grant-in-Aid of Research from Sigma Xi, the Scientific Research Society, to J.W. CHESS is supported by a grant from the National Science Foundation (DMR 90-21700).

21 April 1992; accepted 11 August 1992

Submicrometer Intracellular Chemical Optical Fiber Sensors

Weihong Tan, Zhong-You Shi, Steve Smith, Duane Birnbaum, Raoul Kopelman*

A thousandfold miniaturization of immobilized optical fiber sensors, a millionfold or more sample reduction, and at least a hundredfold shorter response time, all simultaneously, were achieved by combining nanofabricated optical fiber tips with near-field photopolymerization. Specifically, pH optical fiber sensors were prepared with internal calibration, making use of the differences in both fluorescence and absorption of the acidic and basic dye species. The submicrometer sensors have excellent detection limits, as well as photostability, reversibility, and millisecond response times. Successful applications include intracellular and intraembryonic measurements. Potential applications include spatially and temporally resolved chemical analysis and kinetics inside single biological cells and their substructures.

Chemical concentration gradients and spatial heterogeneities are of great interest in many areas, including analytical chemistry, cell biology, physiology, toxicology, and materials science. In cell biology, for example, intracellular measurements could produce concentration profiles of cytoplasms. Probes of very small size are needed to make such measurements. In this report, we describe a technology that enables the development of optical fiber sensors with submicrometer to tens of micrometer dimensions and extremely short response times. These sensors serve as nonperturbative probes for the measurement of microscopic and submicroscopic chemical profiles and their time development.

Electrically based sensors with submicrometer dimensions and subsecond response times have been used to probe chemical concentrations that are spatially heterogeneous (*1*). However, this is not the case for optical fiber sensors, which have been widely used in recent years (*2–4*) and have demonstrated several advantages over electrically based sensors (*2–3*). The most important disadvantage has been the absence of an optical fiber sensor small enough to probe spatial, chemical, or biological heterogeneities in the submicrometer size range. The smallest optical fiber sensor reported to date is about 100 μm, requires a sample volume of microliters, and has a response time of several seconds. We have developed an optical fiber sensor for spatially heterogeneous measurements, with sizes as small as 0.1 μm and sample volume requirements on the order of femtoliters. At the same time, these new optical fiber sensors are also capable of fast (millisecond) monitoring of chemical and biological reactions, for example, chemical kinetics inside restricted intracellular domains, where nonclassical rate laws apply (*5*).

There are two major difficulties in making small-sized optical fiber sensors. One is the limitation in most of the available techniques for the attachment of chemicals or biological reagents to the fiber surface. The attachment of chemical or biological reagents by membranes or tubing or any other mechanical method makes only very limited use of the fiber tip surface, which results in very weak signals and very slow response times. The covalent immobilization of reagents by photopolymerization on the distal end of an activated fiber has solved this problem (*3, 4*). In this approach, the polymer serves to increase the surface area, which results in multiple reagent immobilization sites. Because there is no need for the use of a membrane or other mechanical means of confinement, the response is faster and the manufacturing is easier. The second difficulty in fabricating small optical fiber sensors is that there are no optical fibers of sufficiently small size commercially available. The smallest optical fiber sold commercially is still in the

Department of Chemistry, University of Michigan, Ann Arbor, MI 48109.

*To whom correspondence should be addressed.

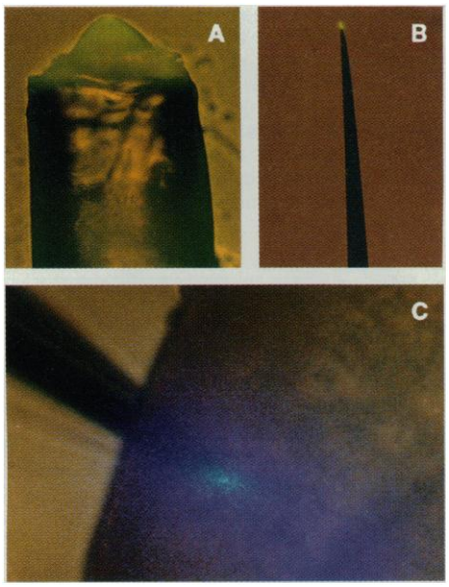

Fig. 1. (**A** and **B**) Photographs of 105-μm and submicrometer optical fiber pH sensors, respectively [magnification in (B) is twice that in (A)]. In (A), the fiber jacket has been taken away, and only the cladding and core are shown. The synthesized polymer at the fiber tip is smaller than the cladding. (**C**) Optical fiber sensor is inserted into the extraembryonic cavity of the rat embryo. Blue light emanates from the sensor.

range of 100 μm (cladding diameter). However, optical fibers can be drawn to very small diameter tips (6–8). We have prepared submicrometer optical fiber chemical sensors as small as 0.1 μm in diameter. We formed aluminum-coated fiber tips and then incorporated a pH-sensitive dye into a copolymer that is attached covalently to the silanized fiber tip surface by photopolymerization.

We notice that calibration of these sensors could be complicated and reproducibility could be a problem for most samples if absolute light intensity measurements were used for pH determinations (the general practice for most ordinary optical fiber sensors). Also, because these optical fiber sensors are very small, there is only a small amount of fluorophore available for sensing. Thus, any significant photobleaching could reduce the accuracy of the measurement. Similarly, the geometry for signal collection could be very critical if absolute intensity measurements were used. These problems were overcome by internal calibration.

With the aim of enhancing the working ability of the miniaturized optical fiber sensors, we used several internal calibration methods to quantify pH that seem to be simpler and apparently better than previously reported approaches (*9*, *10*). Our method is based on the fluorescence intensity ratio obtained from different wavelengths of the same emission spectrum for a single dye. It is highly effective for small-sized sensors, especially when the absorption differences of dye species are also used. Because one can obtain various ratios by selecting the intensities at different wavelengths of the same spectrum, this approach gives more than a double check for a single experiment. The dynamic range can be increased up to ten times if two different excitation sources are used. Thus, our method greatly enhances the sensitivity and accuracy of our measurements and greatly improves the working ability of these miniaturized sensors in biological samples.

For clarity, we note the common misconception about optical techniques being limited by the diffraction limit to about $\lambda/2$, where λ is the wavelength of light. Although this is true for most conventional optical applications, it does not apply to near-field or other scanning probe techniques (6–8). Furthermore, with the use of exciton-optical techniques (*11*, *12*), the miniaturization is limited only by the size of the molecular probe.

The construction details have been given elsewhere (*13*). In this report, the important procedures are briefly discussed. Optical fiber tips have been used as scanning probes in near-field scanning optical microscopy (NSOM) (6–8) and molecular exciton microscopy (*7*, *11*, *12*). The apparatus consists of a micropipette puller and a CO_2 laser. One produces the fiber tip by drawing an optical fiber in the puller with the use of appropriate program parameters and by heating from a CO_2 infrared laser. Optical fibers can be tapered to well below 0.1-μm tips, hereafter referred to as pulled tips. These pulled fiber tips are coated with aluminum, leaving the end face as a transmissive aperture. To make the pulled tip into a light source, we optically couple a laser beam into the opposite end of the pulled tip.

We prepared optical fiber sensors of various sizes, ranging from submicrometer to tens of micrometers, by incorporating a derivative of fluoresceinamine, *N*-fluoresceinylacrylamide (FLAC), into an acrylamide and *N*,*N*-methylenebis(acrylamide) copolymer that is attached covalently to a silanized fiber tip surface by photopolymerization (*4*, *13*). For most of our submicrometer sensor work, photopolymerization was used, although thermal polymerization was also tried. The key difference between these methods is that by photopolymerization the sensor size is controlled by the area from which the light exits, whereas for thermal polymerization the size cannot be controlled in this way. Light and heating were combined for photopolymerization. The thickness of the polymer on the fiber tip was

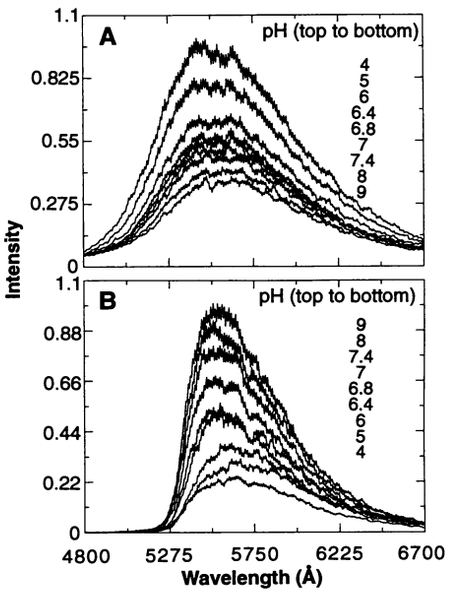

Fig. 2. Fluorescence emission spectra of optical fiber sensor at 25°C. (**A**) Excitation at 442 nm. (**B**) Excitation at 488 nm.

controlled by the reaction time allowed for the polymerization on the fiber tip and was smaller than or close to the size of its diameter (*13*).

We collected the signal through the objective lens of a microscope, which increases the collection efficiency by one or more orders of magnitude compared to back collection (through the same fiber). For the smaller diameter sensors, a new apparatus was built. An Olympus inverted frame fluorescence microscope was connected with either an optical multichannel analyzer (OMA) or a photomultiplier tube (PMT). A 488-nm Ar^+ or a 442-nm He-Cd laser beam was used for excitation of the dye polymer.

The multi-mode and single-mode endstructure of the pulled fiber tapered uniformly from the original fiber to a submicrometer tip with a flat end-surface perpendicular to the fiber axis (Fig. 1B). Whereas the sides of the tip were coated with aluminum, the flat end was left bare, and a tiny aperture was formed. When a 30-mW, 442-nm laser beam was coupled into the aluminum-coated fiber tip, a very bright spot at the tip could be seen under the microscope. This probe delivered light very efficiently to the aperture because all the radiation remained bound to the core to within a few micrometers from the tip. The signal emerging from a randomly chosen 0.2-μm fiber tip (blank) was 10^{12} photons per second, as measured by neutral density filters. Scanning electron microscopy showed that the diameters of the fiber tips were from 0.1 to 1 μm, and most were about 0.5 μm. We have made smaller tips in our NSOM research (*7*), and the smallest fiber tip report-

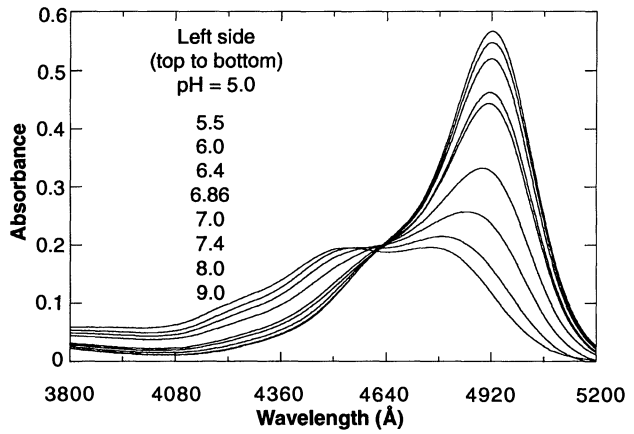

Fig. 3. Absorption spectra of FLAC monomer solution for different values of pH at 25°C.

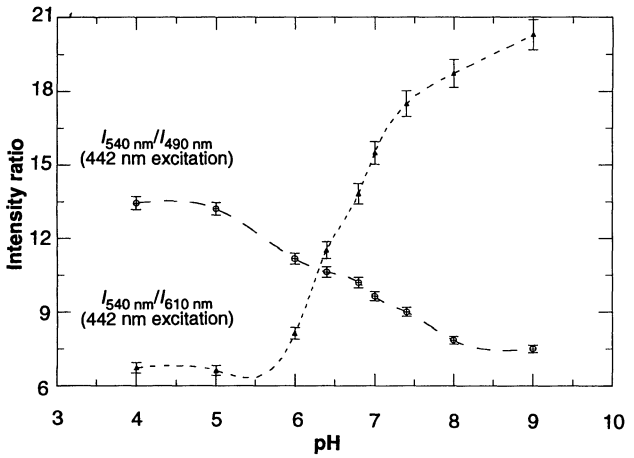

Fig. 4. Fluorescence intensity ratios versus pH at 25°C (from both 442-nm and 488-nm excitation spectra).

Table 1. Measurements of the pH of aqueous samples. The first line gives the measured intensity ratios (that is, the intensity at 540 nm divided by that at 610 nm, both resulting from excitation at 488 nm). Using these ratios and a calibration curve that had been obtained separately, we derived pH(1) values. The pH(2) values were obtained directly from the commercial bench-top pH meter.

Measurement	Sample			
	A	B	C	D
$\frac{I_{540}}{I_{610}}$	12.37	11.89	10.78	9.13
pH(1)				
pH(2)	7.20	7.00	6.70	6.30
Error (pH)	+0.05	+0.07	−0.08	+0.05

Table 2. Enhancement of the fluorescence intensity ratio. Two fluorescence spectra of the sensor were obtained by excitations at 442 and 488 nm, respectively. Two intensities at two different wavelengths of these spectra (one from each spectrum) were used to calculate the intensity ratio as $I_{540nm/488nm}/I_{610nm/442nm}$. The ratio differential is defined as, for example, the intensity ratio at pH 9 divided by that at pH 4 for the pH range from 4 to 9.

pH range	Ratio differential		Enhancement (%)
	$\frac{I_{540/488}}{I_{610/488}}$	$\frac{I_{540/488}}{I_{610/442}}$	
4 to 9	3.01	7.03	230
7 to 8	1.31	1.84	140

ed (6) is about 0.02 μm in diameter.

For comparison, larger size (100 to 200 μm) unpulled fiber sensors were also prepared by photopolymerization on the silanized fiber surface. The polymer grew only on the fiber core surface where light is emitted. The fine structure of the polymer was quite clear. Results of pH testing on this sensor were comparable with those from previous studies (*13*).

To fabricate the submicrometer sensor, we had to optimize the reaction temperature, polymerization time, and laser power, as well as the coupling efficiency of the sensor in order to grow submicrometer-size polymer probes on the fiber tip surfaces. No fine structure of the probe at the fiber tip could be seen because of the resolution limitations of conventional optical microscopes. When we viewed the sensor under the microscope, only a small and unresolved light spot was seen at its tip, which supports our claim that a submicrometer-size sensor has been fabricated (Fig. 1B).

Fluorescence spectra of the sensor for two excitation wavelengths are shown in Fig. 2. The dependence of the fluorescence intensity on pH was inversely related to the magnitude of the excitation wavelength. For excitation at 442 nm, higher pH decreased the fluorescence intensity, whereas for excitation of 488 nm, higher pH increased the fluorescence intensity. This effect is a consequence of the isosbestic point in the absorption spectra (Fig. 3).

Submicrometer pH fiber sensors were tested with nine different buffer solutions, from pH 4 to 9. Measurements were cycled several times between these values of the pH. For each pH buffer solution, a fluorescence spectrum of the sensor was recorded by the OMA system. The typical exposure time for taking the fluorescence spectrum was 0.5 to 10 s for submicrometer sensors. The use of the OMA system, compared to that of monochromator or optical filters, greatly enhanced the efficiency and precision of the experimental results. Moreover, because very short sensor excitation times were used, no evidence of photobleaching was observed after repeated experiments over a long time period. Thus, the lifetime of the sensor had been prolonged. We estimate that as far as bleaching is concerned, a given sensor can be used for tens of thousands of measurements (see below).

Figure 4 shows the useful ratios for each excitation obtained at three different wavelengths from a typical sensor that we have constructed. The ratio of the intensities at two different wavelengths can be used to quantify pH. Other ratios can be used, if necessary. The ratios at 540/490 nm and at 540/610 nm are large enough for a sensor to measure pH sensitively in the physiological range. Only certain wavelength combinations give accurate calibration. Moreover, different sensors have slightly different behaviors for their intensity ratios, probably as a result of the sensor geometry or dye distribution (aggregation).

The feasibility of the miniaturized optical fiber sensor and of the internal calibration technique has been tested with some aqueous solutions and several biological samples. The biological samples tested were blood cells, frog cells, and rat embryos during various ages of their early life (from 8 to 12 days) (*14*). In Fig. 1C, we show the pH measurement of a mid-gestation rat embryo. The optical fiber sensor was inserted into the extraembryonic cavity of the embryo. Thus, we need only a single embryo to measure pH, whereas previously up to 1000 embryos had to be "homogenized" for a single measurement (*15*). Our single embryo pH measurements (for example, pH

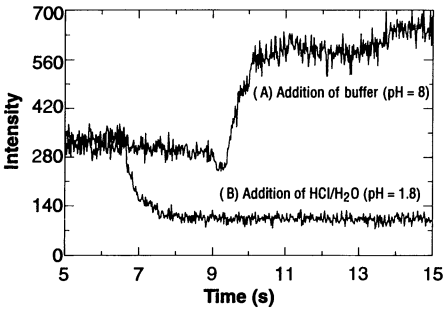

Fig. 5. Response time experiments at 25°C. The sensor (~80 μm) was first kept in air. During data acquisition, a pH 8 buffer was added to the container with the sensor (curve A). For curve B, a solution of HCl-H_2O (pH 1.8) was added to a container in which the sensor was immersed in a pH 6.86 buffer solution. Excitation at 488 nm was used for both experiments.

7.50 ± 0.05 for day 10 rat embryo) agree with those from "homogenized" samples (for example, pH 7.46 ± 0.06 for day 10 mouse embryos). Furthermore, the measurements carried out by our sensors are nondestructive single-cell operations. A complete embryo study will be reported (*16*).

Using four aqueous solutions in the physiological pH range (Table 1), we compared the accuracy of these optical fiber sensors to that of a macroscopic standard high-precision pH meter (Omega). The results from the sensor are similar to those obtained from the commercial pH meter and demonstrate the effectiveness of the internal calibration method in quantifying pH.

Because of the opposite effects of pH on absorptivity at different wavelengths (Fig. 3), we made use of the differences both in absorption and in fluorescence of the dye at different wavelengths to quantify the pH and increase the differential in intensity ratio per pH unit change. We obtained a significant enhancement factor (Table 2).

The miniaturization of the sensor also permits a very fast response time because the analytes have immediate access to the dye on the sensor tip. The submicrometer sensors have response times shorter than can presently be measured (20 ms). This is consistent with Fig. 5, which shows the 10 to 90% response times for one of our largest sensors (~80 μm) to be ≤500 ms.

The submicrometer pH sensor has a detection limit of ≤3000 hydrogen ions in the measurements of pH 8 buffer solutions inside a micrometer-size membrane hole (*13*). The submicrometer pH sensor also has good stability, even when a high laser power (30 mW, collected fluorescence intensity around 10^5 counts per second) is used. Over a time period of 40 min, only a 10% loss in intensity for sensors immersed inside a buffer solution was recorded. The photobleaching is practically imperceptible at the routine lower laser power operation.

REFERENCES AND NOTES

1. M. A. Arnold and M. E. Meyerhoff, *CRC Crit. Rev. Anal. Chem.* **20**, 145 (1988).
2. W. R. Seitz, *Anal. Chem.* **56**, 16 (1984); *CRC Crit. Rev. Anal. Chem.* **19**, 135 (1988).
3. O. S. Wolfbeis, *Fiber Optic Chemical Sensors and Biosensors* (CRC Press, Boca Raton, FL, 1991), vol. 1.
4. S. M. Barnard and D. R. Walt, *Nature* **353**, 338 (1991); C. Munkholm, D. R. Walt, F. M. Milanovich, S. M. Klainer, *Anal. Chem.* **58**, 1427 (1986).
5. R. Kopelman, *Science* **241**, 1620 (1988).
6. E. Betzig, J. K. Trautman, T. D. Harris, J. S. Weiner, R. L. Kostelak, *ibid.* **251**, 1468 (1991).
7. R. Kopelman *et al.*, *SPIE J.* **1637**, 33 (1992).
8. A. Lewis and K. Lieberman, *Anal. Chem.* **63**, 625 (1991).
9. L. M. Christian and W. R. Seitz, *Talanta* **35**, 119 (1988); Z. Zhang and W. R. Seitz, *Anal. Chim. Acta* **160**, 47 (1984).
10. S. Luo and D. R. Walt, *Anal. Chem.* **61**, 174 (1989).
11. K. Lieberman, S. Harush, A. Lewis, R. Kopelman, *Science* **247**, 59 (1990).
12. W. Tan, R. Kopelman, K. Lieberman, A. Lewis, in *Dynamics in Small Confining Systems*, J. M. Drake, J. Klafter, R. Kopelman, Eds. (Materials Research Society, Pittsburgh, PA, 1990), pp. 195–198.
13. W. Tan, Z.-Y. Shi, R. Kopelman, *Anal. Chem.*, in press.
14. C. Harris, *Teratology* **43**, 229 (1991).
15. H. Nau and W. J. Scott, *Arch. Toxicol.* (suppl. 11), 128 (1987).
16. W. Tan, B. A. Thorsrud, C. Harris, in preparation.

17. We thank B. Thorsrud and C. Harris for providing rat embryo samples and S. Parus for computer programming. We also thank M. Meyerhoff, M. Morris, M. Shortreed, and D. Walt for helpful discussions. Supported by Department of Energy grants DE-FG02-90ER 60984 and DE-FG02-90ER 61085.

5 June 1992; accepted 14 August 1992

Large Enhancement in Oxygen Mobility in the Superconductors $RBa_2Cu_3O_7$ with Increasing Rare-Earth Size

J. L. Tallon and B.-E. Mellander*

Ultrasonic composite oscillator measurements of the mechanical relaxation in $RBa_2Cu_3O_{7-\delta}$ arising from oxygen hopping in the basal chain layer show enhancements in oxygen mobility of 20, 50, and 100 times for R = gadolinium, neodymium, and lanthanum, respectively, above that for R = yttrium. The use of the larger rare earths offers a practical solution to the major problem of slow oxygen diffusion in single crystals and bulk, dense material for wires and melt-textured monolithic bodies.

Solid-state oxygen diffusion is of interest in a range of disciplines and technologies from diffusion in minerals for geothermometers and geobarometers (*1*), to fast oxygen ion conductors for fuel cells and oxygen sensors (*2*), to electronic ceramics (*3*), to cuprate superconductors with high superconducting transition temperatures, T_c (*4*). The 90 K superconductors $RBa_2Cu_3O_{7-\delta}$ (R = Y, La, Nd, . . .) are oxygen-deficient ($\delta > 0.7$) as synthesized and, as a consequence, insulating. An essential step in their manufacture is to load oxygen after synthesis by annealing or slow cooling in O_2 to 350°C to induce superconductivity. The transition temperature is maximized at about 90 K when oxygen deficiency is more or less eliminated and $0 \leq \delta \leq 0.1$. Oxygen diffusion into and through the lattice occurs in the basal chain layer between the ideally occupied O1 site and the ideally unoccupied O5 site. This incorporation of oxygen presents no difficulty in conventionally prepared materials in which, because of their high porosity (>15%) and microcracks, oxygen is able to diffuse rapidly into the material bulk. Moreover, because of the $T_c \approx 90$ K plateau (*4*), incomplete oxygen loading may result in a 90 K superconductor, although other properties, such as flux pinning, will not be optimized.

Dense, bulk material presents a rather different picture. Because the oxygen self-diffusion coefficient between 400° and 500°C is in the range 10^{-12} to 10^{-11} cm^2/s, the rate of oxygen loading in $YBa_2Cu_3O_{7-\delta}$ (1-2-3) may be prohibitively slow for samples that are more than 98% dense and several millimeters in dimension (*5*). In addition, the markedly anisotropic thermal strains (*4*) that occur on oxygen loading (positive in the *b* direction and negative in the *a* direction), as well as the effects of inhomogeneous oxygen loading, result in differential stresses that cause substantial microcracking. This change in microstructure, of course, has a harmful effect on critical current density and on mechanical properties.

It was earlier shown (*6*) that, by substituting A = Na, K, or Ca into 1-2-3 according to the formula $Y_{1-x}Ba_{2-y}A_{x+y}Cu_3O_{7-\delta}$ ($x + y$

New Zealand Institute for Industrial Research and Development, Post Office Box 31310, Lower Hutt, New Zealand.

*Permanent address: Department of Physics, Chalmers University of Technology, Gothenburg, Sweden.